Desalination and Water Treatment
www.deswater.com

doi: 10.5004/dwt.2020.26432

208 (2020) 386–398
December

Effective removal of carcinogenic dye from aqueous solution by using alginate-based nanocomposites

Azeem Bibi[a], Sadiq-ur-Rehman[a,*], Tasleem Akhtar[b], Muhammad Imran Shahzad[c]

[a]*Department of Chemistry, University of Azad Jammu and Kashmir, Muzaffarabad, Pakistan, Tel. +92 3018086819; emails: srkhattak@gmail.com (S.-u.-Rehman), azeembibi786@gmail.com (A. Bibi)*
[b]*Department of Zoology, University of Azad Jammu and Kashmir, Muzaffarabad, Pakistan, email: seemeawan88@gmail.com (T. Akhtar)*
[c]*Nano Sciences and Technology Department, National Center for Physics, Islamabad, Pakistan, 44000-Islamabad, Pakistan, email: Imran-shahzad@live.com (M.I. Shahzad)*

Received 20 February 2020; Accepted 6 August 2020

ABSTRACT

Significant efforts are applied to prepare novel nanomaterials in which functionalized multi-walled carbon nanotubes (COOH-MWCNTs) are dispersed in alginate-chitosan network under ultrasonic waves. Instrumental techniques like scanning electron microscopy, thermal analysis (thermogravimetric analysis/differential scanning calorimetry), Fourier transform infrared spectroscopy, X-ray diffractometry, and Brunauer–Emmett–Teller are used for characterization of materials. Nanocomposite films are also evaluated based on swelling behavior. These techniques and measurements indicated the interacted and more stable nature of nanocomposites compared to the starting materials. The prepared films are used as sorbents to remove the Congo red dye from the aqueous solution. Various experimental parameters like contact time, temperature, pH, and dosage are varied to explore their effect on adsorption capacity. Nanocomposites films are analyzed for % desorption and recycled in the adsorption process successfully for 12 times. The adsorption mechanism involved is a pseudo-first-order mechanism. While isothermally, the Freundlich model appears to fit better than the Langmuir adsorption model. The high adsorption efficiency with more strength and regeneration suggests nanocomposite films as the best alternative for already existing petroleum-based membranes.

Keywords: Nanocomposites; Alginate-chitosan; Adsorbents; Films

1. Introduction

Unfortunately, the community of this planet is incessantly facing the problem of inadequate clean potable water due to rapid industrialization, increasing urbanization, and environmental changes. These sources insert different unwanted anthropogenic pollutants in the ecosystems [1]. Textiles dyes are placed at the top of the list in all these pollutants and are considered as highly toxic and carcinogenic in nature. From the synthetic dyes, the largest colorants belong to azo groups (60%–70%). These azo dyes are largely used in the coloring of various substrates like synthetic and natural fibers, plastics, leather, paper, mineral oils, waxes, and even with (selected types) foodstuffs and cosmetics [2]. Due to their poor fixation to fabrics, a high concentration of these dyes is estimated in water and ranging from 5 to 1,500 mg/L [3,4]. Congo red is one of the Azo dyes, very stable, less biodegraded, and various health problems such as bladder cancer in humans, splenic sarcomas, cytoplasm anomalies, and chromosomal aberration in mammalian cells are caused by this dye [5]. Therefore, it is very important to treat this industrial effluent before its discharge into freshwater.

* Corresponding author.

Many traditional methods like chemical precipitation [6,7], electrochemical deposition [8], ion exchange, and membrane separation [9] have been applied for the time being to purify the potable water. Over the past several decades, there is a growing interest in the development of new water treatment procedures, where adsorption by various natural and synthetic polymers play a crucial role [10–13]. The preferable demand of the adsorption method is due to its high efficiency, cheap adsorbents, easy handling, enhanced surface area, and availability of different adsorbents [3]. Several natural polymers such as polysaccharides have been suggested to be more efficient because of their low molecular weights, changeable porosity, biodegradability, non-toxicity, and easy availability [14,15].

Alginate is one of the natural polymers, obtained from brown algae and composed of D-mannuronic acid (M) and L-guluronic acid (G) units. It is most plentiful natural polymer, has been reported to react with other materials due to large number of active hydroxyl and carboxyl groups that provide reactive sites and coordination centers for other materials [16]. Sodium alginate dissolves in aqueous solution (by dissolving the sodium ions) and crosslinks with itself as well as with other available ions to form jelly materials. It is biodegradable, biocompatible, renewable, non-toxic, and widely investigated for adsorption studies. However, a potential problem with sodium alginate and its derivatives is poor strength, flexibility, and high hydrophilicity [17,18]. Furthermore, this polymer is fragile in nature, water-soluble, and less stable to use again and again for the removal of dyes. So, it is the utmost need to find any material which improves the strength, insolubility, and porosity of alginate by maintaining the dye adsorbing ability.

Chitosan is a cationic polysaccharide having randomly distributed β-[1 → 4]-linked D-glucosamine and N-acetyl-D-glucosamine units, forms very stable and water-insoluble composites with other materials. It is extracted from crabs, prawns, fungi, and extensively applied for the adsorption process due to film-forming ability, insolubility together with a large number of functional groups. Chitosan is flourished with NH_3 and OH reactive groups that are responsible for intermolecular and intramolecular linkages. The positively charged NH_3^+ groups of chitosan has the ability to react with negatively charged COO^- groups of alginate and strong polyelectrolytic complex is formed at room temperature [3].

Current progress in nanotechnology opens unprecedented opportunities to synthesize cheap and very stable hybrid adsorbents with greater porosity and adsorption capacity by utilizing the synergistic effect of nanoparticles with polymers [3,19]. Due to small size and large surface area, nanoparticles interact strongly with matrix and give very promising properties to the implanted materials. Carbon nanotubes (CNTs) are the nanoparticles that act as best reinforcing materials and have a large surface area, greater chemical reactivity, and high aspect ratio, less chemical mass, and greater strength [20]. Several CNTs based nanocomposites are reported in the literature, in which CNTs are dispersed and immobilized in the polymeric matrix and efficiently used to remove water pollution [18,21,22].

Based on the importance of this work, we combined the synergistic effect of more than one natural polymers in the presence of nanoparticles. As the different polymers are crosslinked with each other, a new variety of sorbents originate with greater functionality, porosity, removal efficiency, reactivity, stability, and recycling property [4,12,23]. Water-insoluble sorbents of alginate with modified porosity are prepared by reacting to the alginate-chitosan blend with COOH-CNTs under ultrasonic waves. These sorbents are then modified into various types depending upon the porosity by adding specific quantity of co-solutes (surfactants), that is, sodium dodecyl sulfate (SDS) and cetyltrimethylammonium bromide (CTAB) are applied for adsorption of Congo red dye. The objectives of this study were to (i) introduce a new water-insoluble nanocomposite films of alginate that contained the stated polymers and nanofillers; (ii) explore the dye adsorption capacity of prepared materials; (iii) evaluate the effect of swelling and porosity on adsorption parameters of synthesized products; (iv) examine the recycling turns in which synthesized composites can withstand and showed encouraging results.

2. Materials and methods

2.1. Materials

Sodium alginate (from brown algae, purity: 98%, CAS number: 9005-38-3, molecule weight: 405.2186 g/mol), chitosan (purity: 99%, ≥75% deacetylated, CAS number: 9012-76-4, molecular weight: 20,000 g/mol), congo red (dye content ≥35%) acetic acid, SDS, cetyltrimethylammonium bromide (CTAB), dimethylformamide (DMF), potassium chloride, calcium chloride (dihydrated), sodium hydroxide, and hydrochloric acid were purchased from Sigma-Aldrich (UK) and used without further purification. MWCNTs were synthesized through chemical vapor deposition [24,25] and were further functionalized through ultra-sonication (37 kHz) to form COOH-MWCNTs [26]. Deionized water was used throughout the procedure.

2.2. Preparation of nanocomposite films

Alginate-chitosan/MWCNTs nanocomposites were synthesized by reacting to the CNTs with alginate having the concentration ratio of alginate (0.9 g) to CNTs (0.016 g) (56:1). An adequate amount of alginate (0.9 g) was dissolved completely in deionized water (40 mL) at 40°C by stirring for 3 h. Chitosan (0.18 g) was separately dissolved in 2% acetic acid (75 mL) solution by stirring for 1 h at 30°C. The COOH-MWCNTs (0.016 g) were dispersed in deionized water (40 mL) in the presence of a trace amount of surfactant (SDS or CTAB) to obtain a clear homogeneous solution. Complete dispersion of MWCNTs was carried out by sonicated the solution for 2 h in a bath sonicator (Elmasonic S 30 H, 50–60H, Japan). Alginate-chitosan/CNTs (Cs90) blend was prepared by sonicated a mixture of alginate (2 mL), chitosan (75 mL), and COOH-MWCNTs (2 mL) dispersed in aqueous solution (containing SDS as a surface-active agent) for further 2 h at 40°C. Similar method was applied to synthesize other blended nanocomposites, for instance, Cc90 (containing CTAB as a surface-active agent), CD90 (no surfactant, CNTs are dispersed in DMF instead of aqueous solution). After 2 h of sonication, the obtained uniform mixture solution was poured into Petri plates and placed for

drying at room temperature. After drying these films were further washed with ethanol and then dehydrated at 40°C in the oven for 5 h. The dried alginate-based films were stored in sealed polyethylene bags for further use.

2.3. Characterization techniques

Advanced instrumental techniques are applied to characterize the nanocomposite films. The surface morphology of nanocomposite films was visualized using scanning electron microscopy (SEM, Joel JSM-6510LV, Japan) and compared with starting materials. The accelerated voltage applied for SEM measurement was 20 kV. The sorts of interactions between components are identified by using Fourier transform infrared spectroscopy (FTIR; Perkin Elmer spectrum 100 series spectrometer, Korea) working in the range of 4,000–400 cm^{-1} at 2 mm/s rate. The thermal stability of composites was determined by thermogravimetric analysis/differential scanning calorimetry (TGA/DSC) techniques using a thermal analyzer (TA SDT Q600) at the temperature range of 0°C–700°C and heat flow –5 to 15 W/g. The surface area and porosity of synthesized materials are visualized by the Brunauer–Emmett–Teller (BET; Quantachrome Nova 2200 e) technique using –0.045 g of the sample at 273 K. The shape, geometry, and pattern of arrangement in polymeric chains were determined by X-ray diffraction (XRD) technique using JDX-3532 diffractometer working at the voltage of 20–40 kV. The X-rays used were of 1.5418 Å to diffract the materials with a scanning range of 0°–160°.

2.4. Measurement of swelling capacity

Synthesized materials were evaluated by swelling ability in neutral water, saline solutions, and in solutions having variable pH. For such evaluation, a specific quantity of sample (14 mg) was dipped in vials containing 100 mL of each solvent. After specific time intervals, the samples were weighted by removing extra surface solutions. This immersion and removing of films in respective solutions take place for that time until an equilibrium swelling was obtained. Swelling capacity was calculated by using Eq. (1) [27].

$$\text{Swelling}\left(\frac{g}{g}\right)=\frac{\left(W_s-W_d\right)}{W_d} \tag{1}$$

Here, W_s is the swollen weights of films at time t and W_d is dry weights of films, respectively.

2.5. Batch adsorption studies

For adsorption studies, an anionic dye Congo red (1 g) was dissolved in distilled water to form a stock solution of dye. Firstly, nanocomposite films were ground to form small pieces of sample to increase the surface area of the adsorbent. For adsorption studies, a known amount (0.020 g) of nanocomposite film was placed in a flat-bottom flask having 25 mL of dye solution (5–700 mg/L) and stirred in a hot plate at 200 rpm for 24 h. The concentration of adsorbate in filtered solution was measured by UV-vis spectrophotometer (UV-1601 SHIMADZU, Korea) and the adsorbed amount can be calculated by using an adsorbing expression. The adsorption capacity and the percentage of dye removal were calculated by using the following mathematical relationships [28].

$$q_t=\frac{\left(C_0-C_t\right)\times V}{W} \tag{2}$$

$$R=\frac{\left(C_0-C_e\right)}{C_0}\times 100 \tag{3}$$

where q_t is the amount of dye (mg g^{-1}) adsorbed at the surface of nanocomposite films, R represents the percentage of dye removal (%), W is the weight (g) of sorbents used, V is the volume (L) of dye solution, and C_0, C_t, and C_e are the concentrations of dye solutions at initial time, at different time intervals, and at equilibrium, respectively.

For kinetic studies, a series of experiments were done by varying contact time from 1 to 240 min at an initial concentration of dye was 50 mg/L. The effect of the adsorbent dose was studied by changing the concentration from 0.02 g to 1.0 g at an initial concentration of adsorbate C_0 = 50 ppm and the contact time was 3 h at 25°C. The relationship between adsorption capacity and adsorbate concentration was also examined by changing the concentration of adsorbate from 5 to 700 ppm. Similarly, for thermal analysis, adsorption experiments were carried out by varying temperatures range from 10°C to 60°C and pH range 2–13 at an initial concentration of adsorbate C_0 = 50 ppm and contact time was 3 h.

2.6. Desorption and regeneration

To study the desorption process, films loaded with adsorbate were washed with distilled water three to four times and put in a flat-bottomed flask having 25 mL of 0.1 molar solution of each from KCl, $CaCl_2{\cdot}2H_2O$, CH_3COOH, HCl, NaOH, and distilled water. The solution in the flask was stirred for 1 h to desorb the adsorbate which was then measured by the UV spectrophotometer. The percentage of desorbed quantity can be calculated as:

$$\%\ D=\frac{M_d}{M_a}\times 100 \tag{4}$$

where M_d is the quantity of desorbing dye and M_a is the quantity of adsorbing dye.

To evaluate the reusability and recycling of samples, the bath experiment is repeated for several times. In a typical procedure, a weighed quantity (0.020 g) of each sample was immersed in a dye solution (50 ppm) and stirred this solution to reach an equilibrium (for 1 h). The color of the dye solution is decolorized after –40–45 min. After reaching the equilibrium adsorption, the adsorbents were separated and rinsed with distilled water to remove the surface dye. Afterwards, the samples were immersed into desorption solution and stirred until the desorption reach balance. Then, the adsorbents were separated from the solution, washed with distilled water, and left to dry for further reusing experiments.

3. Results and discussions

3.1. Characterization techniques

The sorts of interactions in alginate (algi), alginate + chitosan (algi+chito), and alginate + chitosan/MWCNTs (algi+chito/MWCNTs) are determined by FTIR and compared with each other (Fig. 1a). The algi film has only the characteristic peaks of its constituents whereas, nanocomposite films also revealed absorption bands of chitosan and MWCNTs in addition to alginate. A prominent peak at 3,000–2,850 cm^{-1} is attributed to C–H bonds (–CH_3) that appeared in algi, algi+chito, and in nanocomposites. The broadband of H-bonded OH groups at 3,484–3,010 cm^{-1} is present in algi and algi+chito [29]. While, in nanocomposite this band appeared in slightly low intense form, suggesting some sorts of interactions between polymeric matrix and nanofillers. These interactions may be due to the COOH of MWCNTs or by N–H of amide functional groups. The bending vibrations appeared at 1,565–1,550 cm^{-1} correspond to the N–H bond of amide functional groups present in nanocomposite films and absent in starting materials. The presence of MWCNTs in nanocomposite films is confirmed by the C=C stretching frequencies of the graphene sheet that appeared at 1,642–1,641 cm^{-1}. The C–O bond of carbohydrate rings in all composites appeared in the form of an intense peak at 1,031–1,010 cm^{-1}. FTIR spectra of nanocomposites further reveal that in the absence of surfactants (i.e., in CD90) a peek at 1,738 cm^{-1} appears which is attributed to the C=O group of naked COOH-CNTs. While in the case of surfactants, this absorption is absent. It may be due to counterion micelles around CNTs by the addition of surfactants.

The uptake of Congo red by nanocomposites is illustrated by FTIR spectra as shown by Fig. 1b. It is indicated that there are some interactions between dye and nanomaterials. As the presence of Congo red is shown by additional peaks (S=O, N=N) in adsorption spectra of materials. It is further investigated that the interactions of Congo red with nanofillers (CNTs) and polymer matrix are grater in CD90 as compared to Cc90 and Cs90, which appeared in the form of the disappearance of S=O and C–O bonds. These sorts of interactions are also indicated in the form of greater adsorption capacity of CD90 as compared to Cs90 and Cc90.

Surface area, pore volume, and pore width of samples are measured by the BET technique and tabulated in Table 1. From these results, it is indicated that all nanocomposite materials are more porous than the alginate. Furthermore, the nanomaterials containing surfactants are more porous in nature than non-surfactant materials, it may be due to the involvement of co-solutes in polymeric structure and formation of micelles, which give greater porosity to the polymeric structure. However, in CD90 film (do not contain surfactant) has less quantity of pores with greater pore volume and width. So, this type of nanocomposite has a less specific surface area as a specific surface area depends upon pore size as well as the number of pores per gram. Similar results were found by another group of researchers [30]. The more porous and stable nature of synthesized nanocomposite films suggests applying as a selective adsorbent in water purification.

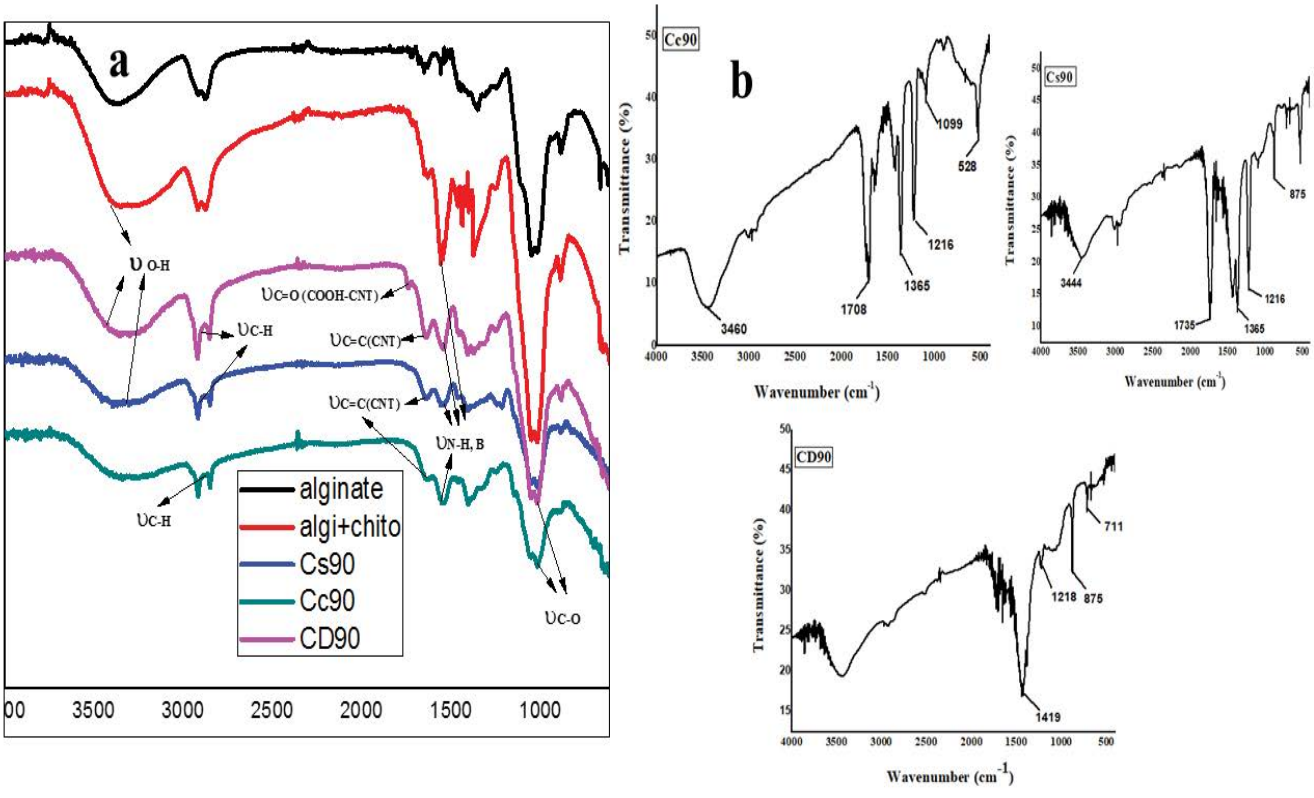

Fig. 1. FTIR spectra of samples (a) before adsorption and (b) after adsorption.

Table 1
Surface area (BET) analysis data of samples

Samples	Specific surface area (m^2/g)	Pore volume (cm^3/g)	Pore width (nm)
Cs90	8.436	0.007	3.179
Cc90	8.195	0.033	3.537
CD90	7.854	0.036	19.902
Algi	0.778	0.236	1.259
Algi+Chito	3.612	0.042	2.162

The thermal behavior of prepared films is analyzed by TGA/DSC and results are indicated in Fig. 2a. It is known from thermal graphs that three types of films (Cs90, Cc90, and CD90) have almost similar behavior at various temperature ranges. The first deflection in mass has appeared at –20°C–70°C which is due to the evaporation of small free molecules, like water, that entrapped in nanocomposites scaffolds. This endothermic evaporation process is also confirmed by depression in DSC curves at a similar temperature. The area of peaks at –20°C–70°C indicates that a very small quantity of water molecules is entrapped due to little availability of free functional groups suggesting greater interactions between functional groups.

The second step of thermal decomposition occurred at about 75°C–195°C. The loss of mass corresponded to this decomposition is exothermic dehydration reaction. Linkages of bonded water break and degradation of carboxylic groups occurred at this temperature [31]. The next predominant stage of thermal decomposition is appeared at about 200°C–400°C. The process of depolymerization, breakage of glycosidic, polyelectrolytic, and interionic electrostatic linkages present between alginate-chitosan and COOH-MWCNTs. The process of deacetylation and deamination in chitosan polymer is also reported in this temperature [32]. On comparison of the thermal stability of alginate-chitosan mixture with the prepared materials, it is known that prepared materials remained stable up to about 400°C, while composite of alginate-chitosan degraded at 300°C suggesting the interactions between polymeric blends and nanofillers [31]. The last step of mass loss attributed to a highly exothermic degradation reaction that occurred at 400°C–570°C. The process of destruction and degradation of mannuronic acid, guluronic acid, and gluconic acid of alginate-chitosan blend lead to the formation of acetic acid, formic acid, and butyric acid along with series of fatty acid is responsible for this mass deflection [33]. The decarboxylation and complete destruction of functionalized CNTs have also occurred at this temperature [31]. At about 570°C complete (100%) thermal degradation occurred.

The amorphous or crystalline nature of synthesized nanomaterials is determined by the XRD technique and results are included in Fig. 2b. Results obtained by these spectra indicate that prepared materials showed an amorphous nature. However, a small level of crystallites and dense packing is also present. The interaction of polymer matrix and nanofillers develop some sort of arrangement pattern in the constituents and crystallites may develop. These crystallites are indicated in the form of some peaks in corresponding spectra. For instance, the Cc90 nanocomposite film showed a smaller peak at around $2\theta° = 24°$, 34° Cs90 at about $2\theta° = 35.8°$, 62.8°, and 74.4° and CD90 at $2\theta° = 35°$, 52°, and 63°. These peaks indicate the presence of some crystallites in polymers.

The surface morphology of prepared samples having surfactants and without surfactants is examined by SEM analysis (Figs. 3a–e). It is known that the surfaces of films without nanofillers (algi and algi+chito) have smooth surfaces. While the films of nanocomposites having polymeric matrix and nanofillers showed different surfaces containing the images of dispersed nanoparticles. From the SEM analysis, it is also investigated that solvating media did not affect the dispersion, that is, two dispersing media showed almost similar behavior of dispersion. Additionally, drying, washing, and film-forming procedures did not disturb the uniform distribution of CNTs in algi+chito matrices, thus give the indication of strong interactions between polymeric matrix and nanofillers [18, 34]. The images of opaque objects which appeared in the form of agglomerated particles are in fact undissolved matrix particles.

3.2. Swelling measurement

Prepared nanocomposites films are evaluated with respect to swelling behavior and compared with starting materials. The results of swelling behavior are included in Fig. 4. It is known that in distilled water, synthesized nanocomposites showed lower swelling values than the algi and algi+chito and is attributed to the sign of utilization of hydrophilic functional groups by the CNTs particles. The interaction between nanofillers and polymeric materials are also confirmed by the stability of nanocomposite films, while the starting materials are fragile in nature. Nanocomposite films also showed a different nature from the staring materials at variable pH and at various saline solutions.

In changing the pH from acidic to basic followed by neutral, swelling capacity also vary and appeared as decreased form in acidic and basic medium while maximum in neutral pH. Protonation of COOH, NH_3, and OH groups in acidic pH and screening effect of counter ions in basic pH squeeze the polymeric chains, and as a result swelling capacity decreased. While in neutral pH, deprotonation of COO^- ions and non-perfect anion-anion (COO^-) repulsion caused the polymeric chains to swell [16].

Charge density of various ions effects on swelling behavior of synthesized materials. It is noted that ions of external solution did not screen appreciably the functional groups of nanocomposites which is explained on the attribution to inherent crosslinking of COOH-MWCNTs with polymeric

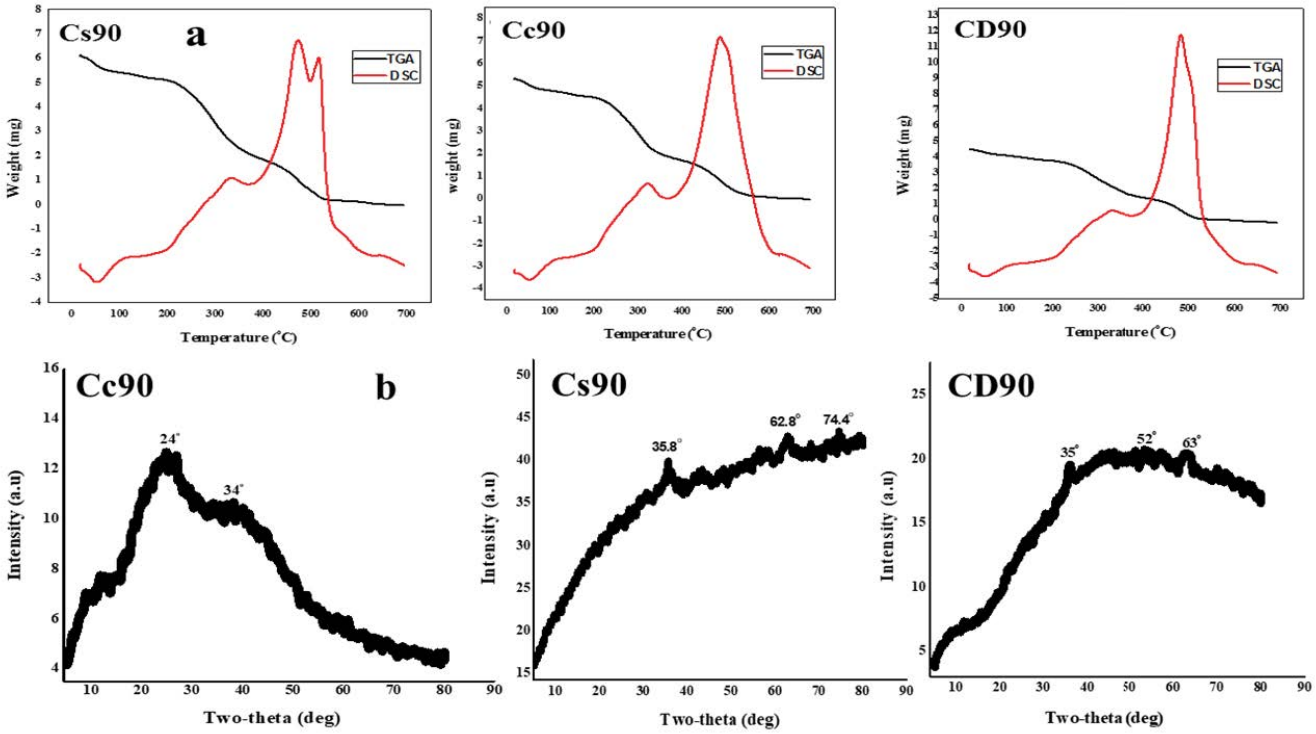

Fig. 2. (a) TGA and DSC graphs of nanocomposites and (b) XRD spectra of nanocomposites.

matrix compared to starting materials. Effect of divalent ions (Ca^{+2}) to react with polymeric chains is greater than monovalent (K^{+1}) and trivalent ions (Fe^{+3}, Bi^{+3}). It may be due the formation of egg-box model formed in alginate gel by incorporation in alginate-chitosan framework [16].

3.3. Adsorption of dye

In this study, prepared films were applied to adsorb Congo red from aqueous solution. The adsorption capacity of synthesized films was evaluated by changing the parameters like contact time, the effect of pH, temperature, and dosage of adsorbate as well as of adsorbent. The effects of these factors are illustrated here.

3.3.1. Effect of contact time

The adsorption capacity of prepared samples with respect to time is shown in Fig. 6a. The obtained values of nanocomposites were compared with starting materials, that is, algi and algi+chito. The maximum adsorption capacities were 40.1 and 39.89 mg/g for algi and algi+chito, while for Cs90, Cc90, and CD90 these values lie in the range of 53.45, 50.77, and 55.34 mg/g, respectively. It is illustrated from experimental data that adsorption of Congo red dye is very rapid in the initial stages of experiment and on reaching the equilibrium, the process of adsorption becomes constant. The attainment of equilibrium is explained by the presence of a large number of active centers at the surface of nanomaterials, and at equilibrium fully saturation of these centers takes place. In this study, the optimum time examined to obtain the equilibrium for algi was ~80 min, algi+chito was ~130 min and for samples (Cc90, Cs90, and CD90) were ~240 min, respectively. The algi and algi+chito films are disintegrated after 80 and 130 min, respectively and all adsorbed dye desorb in water, while the synthesized films remained stable after 240 min. Additionally, the maximum adsorption of Congo red was achieved by CD90 (55.34 mg/g) which is maybe due to maximum interactions between dispersed CNTs and dye and by uptake of wide pores [35]. The next highest value is of Cs90 (53.45 mg/g) and Cc90 showed adsorption capacity in the range of 50.77 mg/g. These relatively lower values of adsorption of films having surfactants are may be due to the narrow pore size and embedded nature of CNTs by micelles and as a result, bonds between the graphene sheet and Congo red are weakened. When Congo red dye adsorbs on the surface of nanocomposite films, the possible sorts of interactions between adsorbate and adsorbent are represented by Fig. 5.

To determine the maximum adsorption capacity of prepared materials and the mechanism of adsorption involved in this process, two models are involved. These are pseudo-first-order and pseudo-second-order kinetic models. The basic assumptions of pseudo-first-order are that the rate of adsorption is proportional to the number of available sites. While pseudo-second-order based on a hypothesis that the adsorption rate is proportional to the number of square roots of vacant sites. The applied kinetic and adsorption models' equations are shown in Table 2. The fitness of the applied model in adsorption capacity of prepared samples depends upon the value of the correlation coefficient (R^2) of linear regression. It is obtained from Figs. 7a and b and Table 3 that the theoretical values obtained from pseudo-first-order are

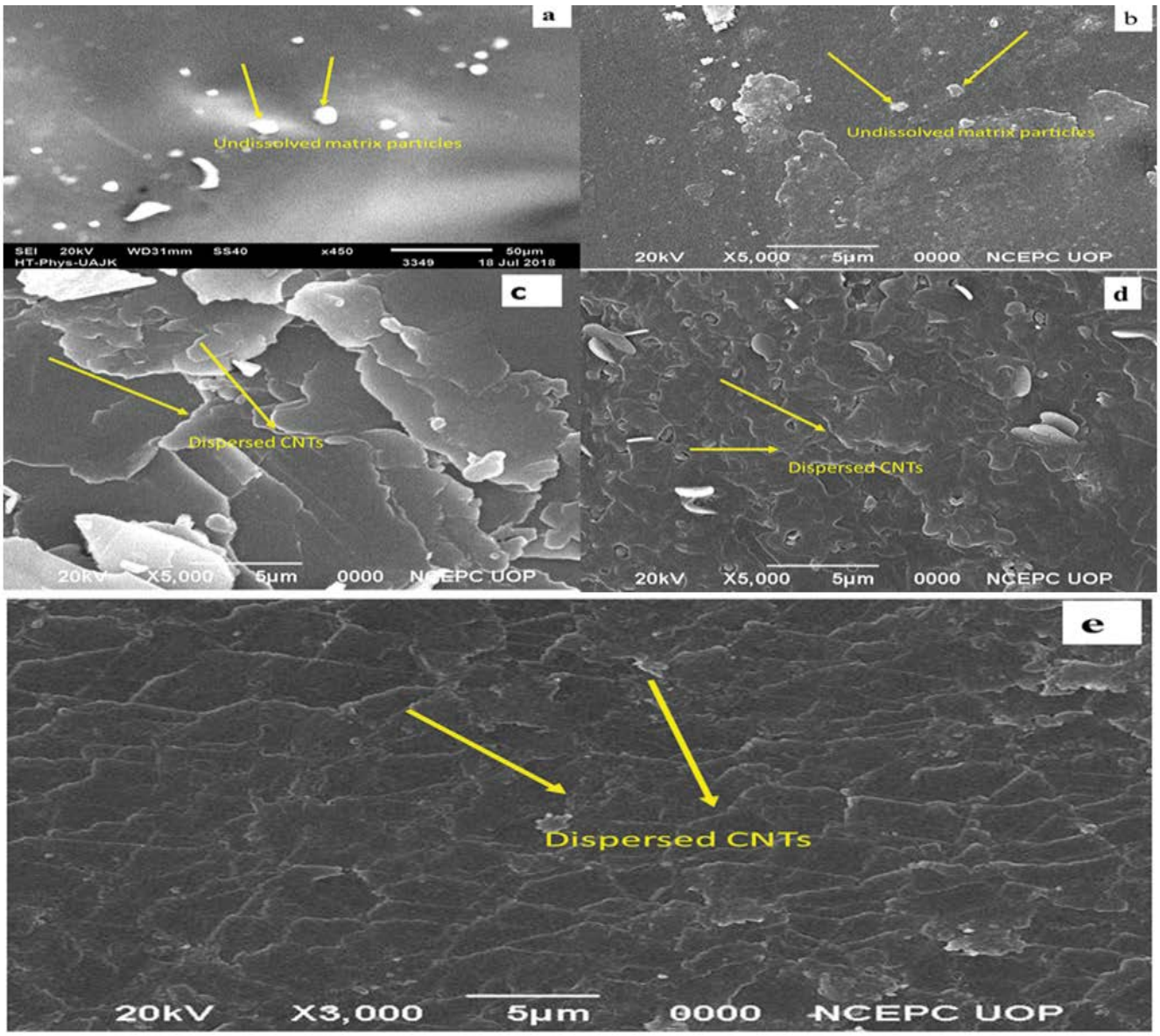

Fig. 3. SEM images of (a) algi, (b) algi+chito, (c) Cc90, (d) CD90, and (e) Cs90 films.

very close to experimental values than pseudo-second-order with greater values of R^2.

3.3.2. Effect of temperature

Temperature also largely effects the adsorption capacity. It is illustrated that increasing the temperature adsorption capacity is increased and results are shown in Fig. 6b. The maximum adsorption capacities of synthesized films reached the values up to 67.11, 63.867, and 60.983 for Cs90, CD90, and Cc90, respectively at 60°C, and up to this limit, the films highly swell and become fragile in nature. These comparatively higher values of adsorption are due to greater mobility of adsorbate at a higher temperature. Furthermore, by increasing temperature, the active sites of adsorbent become more open by increasing activation energy (due to disruption of intermolecular forces) and thus become more accessible for adsorbate [36]. While in the case of algi and algi+chito, the highest adsorption capacity reaches the values of 33.002 and 45.83 mg/g respectively, and films at a lower temperature (40°C) swell and disintegrate. This swelling and disintegration at a lower temperature is an indication of the instability of films because of the absence of nanofillers.

3.3.3. Effect of pH

Adsorption capacity is also varied by changing the pH, it is found that all these films showed similar behavior in acidic, neutral, and basic medium. Synthesized films showed maximum adsorption ability in neutral pH and showed less adsorption capacity in acidic as well as in basic medium. In acidic pH, due to the formation the H-bonding, films collapse, and decrease the surface area, which results in decrease adsorption capacity. In a neutral medium, the protonated

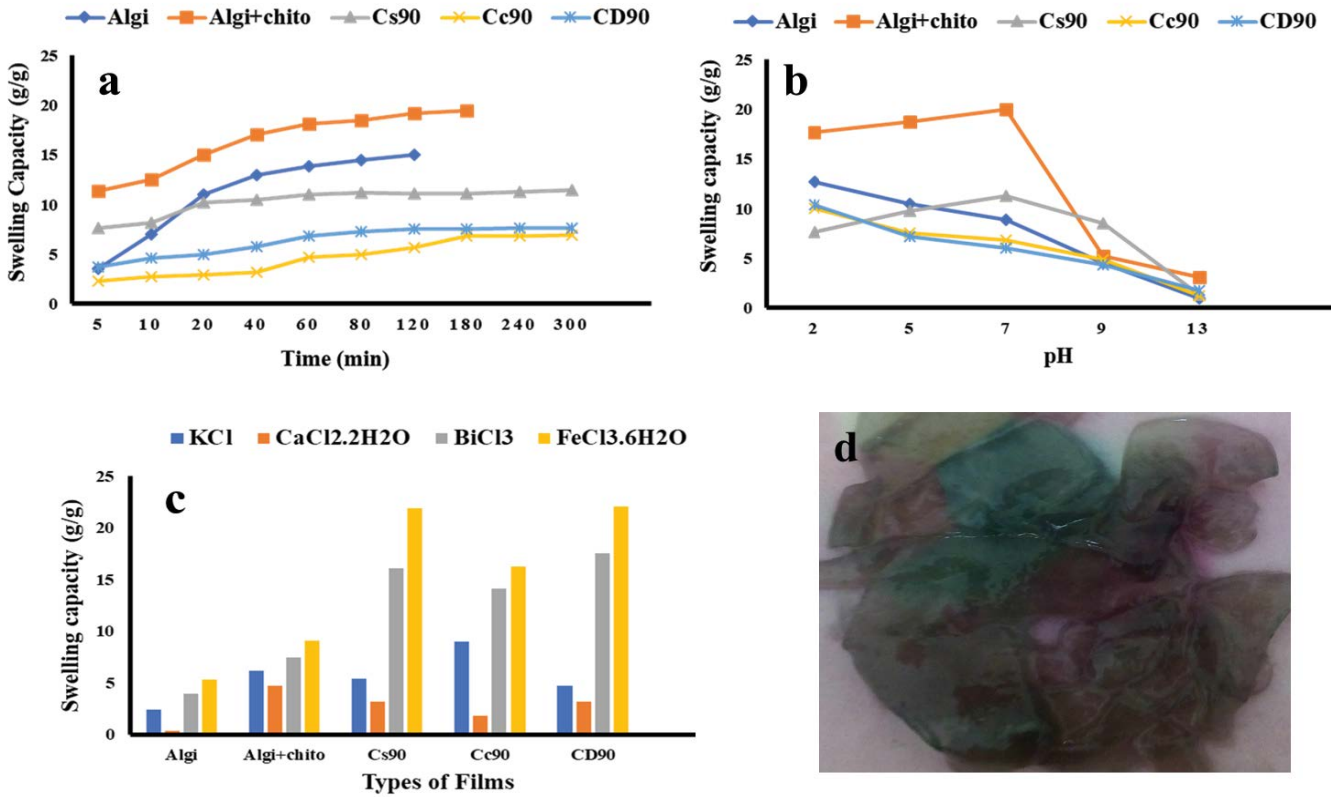

Fig. 4. Swelling behavior of synthesized samples in (a) distilled water, (b) variable pH, (c) various saline solutions and (d) swollen image of Cs90 nanocomposite.

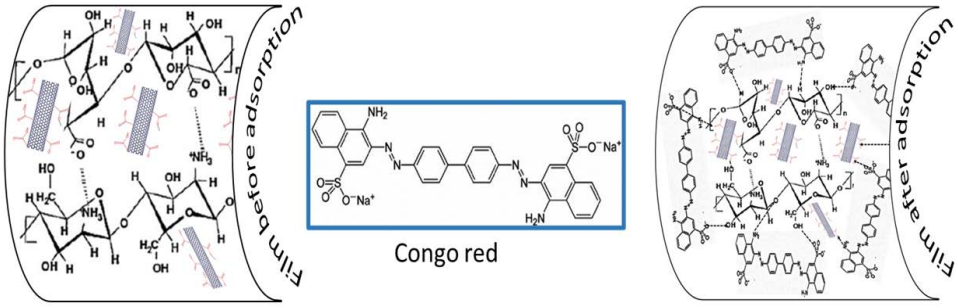

Fig. 5. Adsorption of Congo red on synthesized CD90 film.

Table 2
Applied adsorption kinetic and isotherm models equations

Kinetic models	Linear equations	Plot	Calculated coefficient
Pseudo-first-order	$\ln(q_e - q_t) = q_{e1} - k_1 t$	$\ln(q_e - q_t)$ vs. t	k_1 = –slope $q_e = e^{\text{intercept}}$
Pseudo-second-order	$t/q_t = 1/k_2 q_e^2 + t/q_t$	t/q_t vs. t	k_2 = slope²/intercept q_e = 1/slope
Isotherm models	**Linear equations**	**Plot**	**Calculated coefficient**
Langmuir	$C_e/q_e = 1/q_m K_L + C_e/q_m$	C_e/q_e vs. C_e	K_L = slope/intercept q_m = 1/slope
Freundlich	$\log q_e = \log K_F + \log C_e/n$	$\log q_e$ vs. $\log C_e$	$K_F = 10^{\text{intercept}}$ n = 1/slope

COOH groups ionized, and resulting COO^- groups repel each other and cause expansion. While in basic medium (>8) decrease in adsorption capacity of all the synthesized films is due to the "charge screening effect" [37]. Where counterions (Na^+ ions) surround anions from all the direction, resulting in shrinkage of jell, and adsorption capacity is decreased. The effect of pH on the adsorption capacity of samples is included in Fig. 6d.

Table 3
Kinetic and isotherm parameters for congo red adsorption on prepared samples

Samples	Cs90	Cc90	CD90	Algi	Algi+Chito
Pseudo-first-order					
q_e (cal.) mg/g	106	95	109	88	97
$k_1 \times 10^{-4}$ (1/min)	4.5	5.2	4.7	5.3	5.2
R^2	0.992	0.991	0.995	0.991	0.993
Pseudo-second-order					
q_e (cal.) mg/g	96.64	92.6	99.89	71	80
$k_2 \times 10^2$ (g/mg/min)	1.32	1.30	1.14	1.32	1.29
R^2	0.983	0.87	0.89	0.976	0.973
Freundlich					
K_F	4.23	2.57	3.27	1.053	2.275
n	0.515	0.52	0.532	0.587	0.501
R^2	0.993	0.998	0.997	0.993	0.998
Langmuir					
q_m	138	136	144	123	126
$K_L \times 10^{-3}$	2.6	2.2	2.5	8.9	9.9
R^2	0.829	0.807	0.884	0.941	0.865

3.3.4. Effect of dosage

The effect of concentration of adsorbent and adsorbate on adsorption capacity (mg/g) is also evaluated. The amount of adsorbent is varied from 0.020 to 1 g and the concentration of adsorbate is changed from 5 to 700 mg/L. It is investigated that by increasing the concentration of adsorbent, the removal efficiency is increased but adsorption capacity is decreased (shown in Figs. 6e and f). This decreased value is attributed to aggregation of adsorbent, and consequently, the available adsorption sites may decrease as well due to the adsorption density [38]. While, by increasing the concentration of adsorbate from 5 to 700 mg/L, the adsorption capacity is also increased and reached up to the maximum values (Fig. 6c). This well-known phenomenon can be ascribed to a large number of accessible Congo red near the adsorbent and a high driving force for mass transfer before the adsorption-desorption equilibrium [39]. In the case of algi and algi+chito films, the adsorption capacity lies in comparatively lower values. These lower values are due to the absence of nanoparticles as well as by the fragile nature of films. In fact, the soft and open structures of films do not bear the load of adsorbed dye and as a result, desorption of dye takes place. Furthermore, due to the absence of CNTs, forces of attraction which present between CNTs and dyes are also absent in algi and algi+chito films and hence attachment of dyes is not favorable.

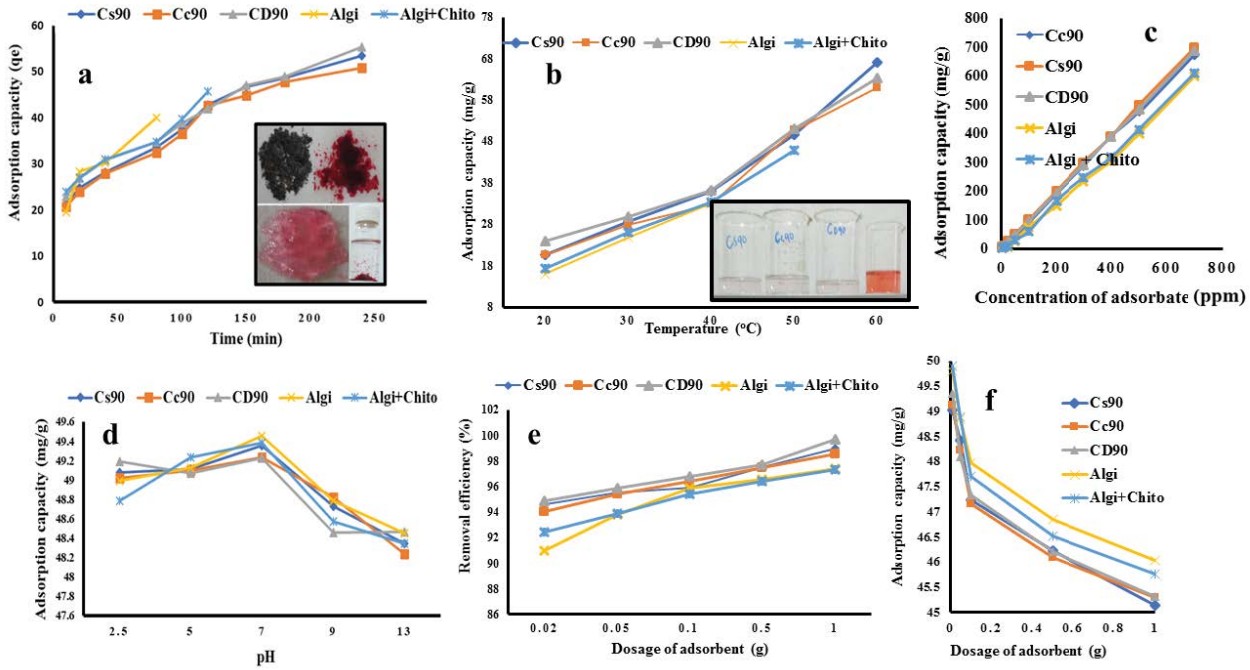

Fig. 6. Effect of (a) contact time, (b) temperature, (c) dosage of adsorbate, (d) pH, and (e and f) dosage of adsorbent on adsorption capacity and removal efficiency of samples.

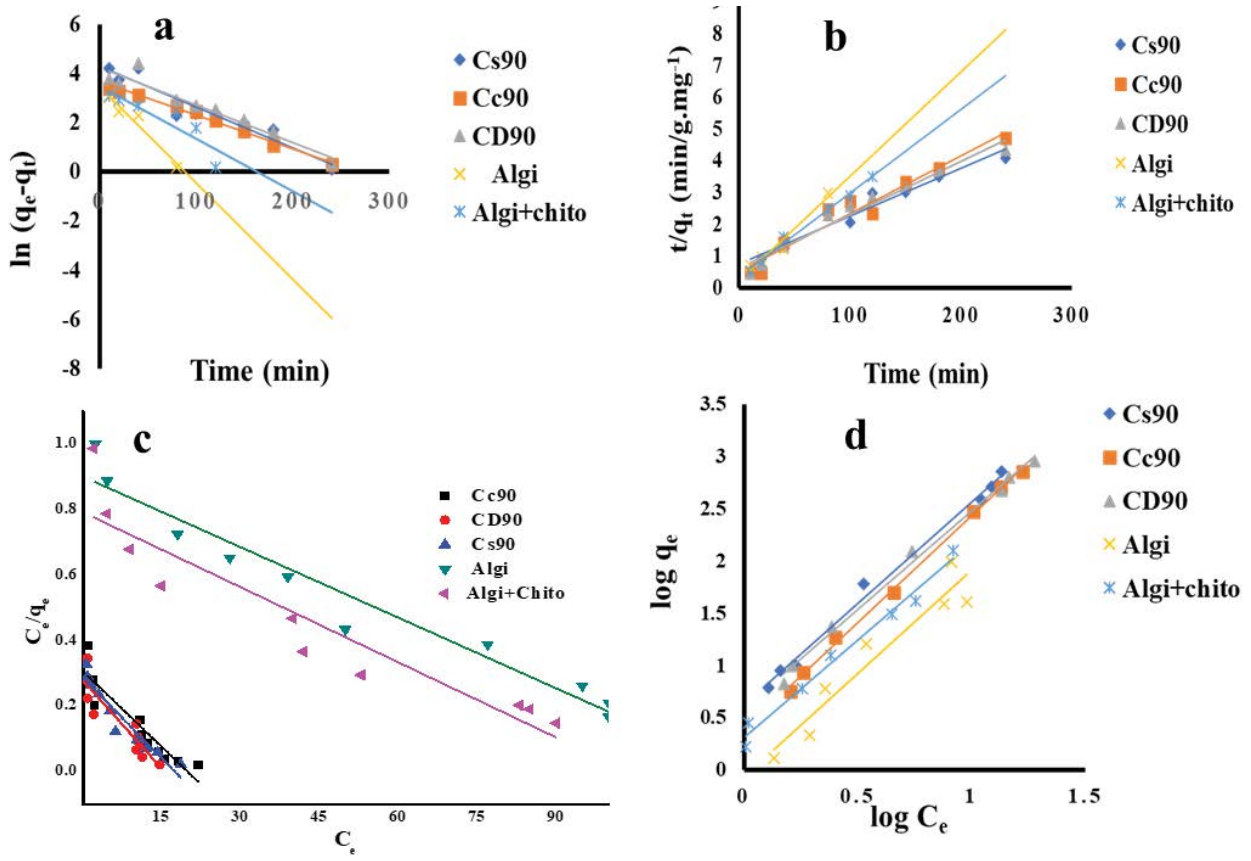

Fig. 7. Linear curve fitting (a) pseudo-first-order, (b) pseudo-second-order kinetic models, (c) Langmuir, and (d) Freundlich isotherms of the adsorption of Congo red on the synthesized samples.

Two adsorption isotherms namely Langmuir model and Freundlich model were used to determine the maximum adsorption capacity of synthesized adsorbents (Figs. 7c and d). Langmuir model assumes that on the homogenous surface, the adsorption process takes place while the assumptions of the Freundlich model based on the heterogeneity of adsorbent. The equilibrium adsorption data applied in two models and results are listed in Table 3. The q_{max} obtained by applying the Langmuir model is 144, 136, 138, 123, and 126 for CD90, Cc90, Cs90, algi, and algi+chito, respectively. However, the correlation coefficient (R^2) from the plot of the Freundlich model is nearly equal to 1, which indicates the best fitting of the Freundlich model with the assumption that the adsorption of Congo red takes place on the heterogeneous surfaces of synthesized materials.

3.3.5. Desorption and regeneration

To obtain a better understanding of the adsorption–desorption mechanism on nanocomposite films and by considering the reusing and recovering of films, sequential desorption experiments were carried out in 0.1 M solutions of each from KCl, $CaCl_2{\cdot}2H_2O$, CH_3COOH, NaOH, HCl, and distilled water. Desorption data for these solvents are illustrated in Table 4. It is shown that, from all the prepared nanocomposites, the best desorption is from CD90. While in the case of films having surfactants (i.e., Cs90 and Cc90), the minimum desorption is from the film having a cationic surfactant (Cc90), while the film having anionic surfactant has intermediate desorbing ability between two extremes. It is also investigated that the maximum desorption is carried by CH_3COOH in each film and the second-highest desorbing value is carried out by HCl. While in the case of deionized water, the desorbing capacity has a minimum value. The highest desorbing ability of CH_3COOH and HCl is may be due to the attainment of new H-bonding between acid and composite film and collapsing of the structure of films which leads to desorb the adsorbed dye [37]. The CD90 film has a maximum desorbing ability which is maybe due to the attainment of new interactions between CNTs and desorbing solvent and as a result, remove the adsorbed dye. As in CD90 the naked and exposed dispersion of CNTs is investigated [37]. While in case of any surfactant, the case is reversed, here, adsorbed Congo red is also linked with surfactant molecules, and maximum desorption does not take place. The presence of counterions also plays an important role in collapsing the films and desorbing capacity is increased. It is investigated that the next highest desorbing values are obtained in the presence of a base (NaOH) which caused charge screening effect and de-swelled the films.

The regeneration and recycling of synthesized films are performed by repeating the bath experiment to determine the reusability of films for dye removing. It is noted

Table 4
Desorption capacity of synthesized materials in the presence of desorbing materials

Types of solutions	Cs90 (%desorption)	Cc90 (%desorption)	CD90 (%desorption)
HCl	79	71	94
NaOH	64	56	83
CH_3COOH	88	67	98
KCl	44	46	47
$CaCl_2$	48	47	50
D. H_2O	18	15	23

Table 5
Number of recycling turns in which synthesized compounds used as sorbents

No. of recycling	Cs90 (mg/g)	Cc90 (mg/g)	CD90 (mg/g)
1	53.8	50.6	54.8
2	53.3	50.6	50.9
3	52.7	51.6	51.8
4	50.6	50.2	50.4
5	54.5	52.3	51.6
6	53.3	50.1	52.3
7	49.2	48.1	53.2
8	50.0	49.0	50.2
9	47.4	49.3	50.3
10	48.4	46.4	49.6
11	48.4	50.4	50.4
12	43.8	48.8	49.7
13	18.6	16.5	19.6

Table 6
Comparison of Congo red adsorption capacities of some other adsorbents

S. No	Type of adsorbents	Maximum adsorption capacity (mg/g)	References
1	*N*,*O*-carboxymethyl-chitosan/montmorillonite	96	[40]
2	Chitosan/CNTs	450	[36]
3	Carbon nanotube/mixed metal oxides	1,250	[34]
4	Graphene oxide/chitosan/silica	294	[38]
5	Xanthan gum/silica	209	[4]
6	Maghemite	208	[2]
7	Mixed iron and aluminum oxide	498	[15]
8	Algi+Chito/CNTs	144	This work

that the synthesized films are successfully applied for 12 times and the red color of dye is completely decolorized for up to eleven times, and for 12th time partially decolorized, which is the indication of the establishment of equilibrium. This attainment of equilibrium is also confirmed by UV absorbance and adsorption capacity measurement. The adsorption capacity of the films for each time is calculated and shown in Table 5. From this data, it is estimated that synthesized films can successfully apply 12 times. After 12th time, composite films remain stable but adsorbing ability is reduced due to the saturation of dyes molecules. On the comparison of synthesized films with starting materials films (i.e., algi and algi+chito), films partly solubilize and disintegrate in the first cycling process. Due to fragile nature, they break and are not used again and again. It is illustrated that; nanocomposites can be used for much more time and do not become fragile due to inherent strength. Furthermore, it is also investigated that a dye that is more concentrated (i.e., 700 ppm) is more adsorbed than a diluted dye solution. Similarly, a film that already adsorbs some

dyes is more efficient (decolorization takes place in lesser time) for further adsorption than the naked film. This behavior is may be due to some sort of wander walls interactions that exist between dye molecules. Similar behavior is also studied by another group of researchers [20].

On the comparison of adsorption capacity of synthesized nanocomposites with reported sorbents (Table 6), it is known that prepared materials are very efficient and eco-friendly sorbents. Although the adsorption capacity is of moderate level, however, their predominance is the number of recycling turns. The recovery of any sorbent is one of the important factors to utilize in industry. Due to the strong polyelectrolytic complex of alginate-chitosan complex, synthesized nanocomposites (Cs90, Cc90, and CD90) having various cavities and channels are successfully applied for 12 times.

4. Conclusion

Very efficient sorbents algi+chito/CNTs nanocomposites are prepared by the greener method in the absence of any crosslinker. Advanced instrumental techniques like SEM, FTIR, XRD, TGA/DSC, and BET are used to determine the morphological, structural, and thermal behavior of nanocomposites. Prepared sorbents are applied for the removal of Congo red from an aqueous solution. Adsorption of Congo red dye on nanocomposite films is examined by the FTIR technique which indicated the dye adsorbed on films. The adsorption capacity (q_m) of prepared nanocomposite materials (Cs90 138 mg/g, Cc90 136 mg/g, and CD90 144 mg/g) increased from starting materials due to the interaction of Congo red dye with CNTs and large surface area (8.4, 8.19 m^2/g, 7.85 m^2/g, respectively) of nanocomposites.

The adsorption kinetics of prepared samples in the adsorption of Congo red dye is consistent of the pseudo-first-order model. Furthermore, based on the correlation coefficient (R^2), the Freundlich model fitted well than the Langmuir isotherm model. Thus, the nanocomposite films are very stable, technically feasible, and cost-effective sorbents that have the potential to use 12 times for removing of the Congo red from aqueous solution.

Acknowledgments

The authors gratefully acknowledge the Dr. Muhammad Zaheer, Department of Chemistry, Lahore University of Management Sciences for BET and TGA/DSC characterizations.

References

[1] M.J. Ascott, D.C. Gooddy, D.J. Lapworth, M.E. Stuart, Estimating the leakage contribution of phosphate dosed drinking water to environmental phosphorus pollution at the national-scale, Sci. Total Environ., 572 (2016) 1534–1542.
[2] A. Afkhami, R. Moosavi, Adsorptive removal of Congo red, a carcinogenic textile dye, from aqueous solutions by maghemite nanoparticles, J. Hazard. Mater., 174 (2010) 398–403.
[3] M.A. Kamal, S. Bibi, S.W. Bokhari, A.H, Siddique, T. Yasin, Synthesis and adsorptive characteristics of novel chitosan/graphene oxide nanocomposite for dye uptake, React. Funct. Polym., 110 (2017) 21–29.
[4] S. Ghorai, A.K. Sarkar, A.B. Panda, S. Pal. Effective removal of Congo red dye from aqueous solution using modified xanthan gum/silica hybrid nanocomposite as adsorbent, Bioresour. Technol., 144 (2013) 485–491.
[5] B.C. Ventura-Camargo, M.A. Marin-Morales, Azo dyes: characterization and toxicity-a review, Text. Light Ind. Sci. Technol., 2 (2013) 86–103.
[6] X. Tang, Z. Li, Y. Chen, Adsorption behavior of Zn(II) on calcinated Chinese loess, J. Hazard. Mater., 161 (2009) 824–834.
[7] H.A. Devrimci, A.M. Yuksel, F.D. Sanin, Algal alginate: a potential coagulant for drinking water treatment, Desalination, 299 (2012) 16–21.
[8] E. Álvarez-Ayuso, A. Garćia-Sánchez, Removal of heavy metals from waste waters by natural and Na-exchanged bentonites, Clays Clay Miner., 51 (2003) 475–485.
[9] Y.S. Ho, G. McKay, A Comparison of chemisorption kinetic models applied to pollutant removal on various sorbents, Process Saf. Environ. Prot., 76 (2009) 332–340.
[10] M.D. Rabiul Awual, T. Yaita, H. Shiwaku, S. Suzuki, A sensitive ligand embedded nanoconjugate adsorbent for effective cobalt(II) ions capturing from contaminated water, Chem. Eng. J., 276 (2015) 1–10.
[11] M. Vesna, R. Vucurovic, N. Razmovski, D.U. Miljic, V.S. Puskas, Removal of cationic and anionic azo dyes from aqueous solutions by adsorption on maize stem tissue, J. Taiwan Inst. Chem. Eng., 45 (2014) 1700–1708.
[12] G. Crini, Recent developments in polysaccharide-based materials used as adsorbents in wastewater treatment, Prog. Polym. Sci., 30 (2005) 38–70.
[13] E.S. Ahmed, H.Y. Moustafa, A.M. El-Masry, S.A. Hassan, Natural and synthetic polymers for water treatment against dissolved pharmaceuticals, J. Appl. Polym. Sci., 131 (2014) 40458–40468.
[14] Y.M. Wang, L. Duan, Y. Sun, N. Hu, J.Y. Gao, H. Wang, X.M. Xie, Adsorptive removal of Cr(VI) from aqueous solutions with an effective adsorbent: cross-linked chitosan/montmorillonite nanocomposites in the presence of hydroxy-aluminum oligomeric cations, Desal. Water Treat., 57 (2015) 10767–10775.
[15] A. Mahapatra, B.G. Mishra, G. Hota, Adsorptive removal of Congo red dye from waste water by mixed iron oxide-alumina nanocomposites, Ceram. Int., 39 (2013) 5443–5451.
[16] K. Norajit, K.M. Kim, G.H. Ryu, Comparative studies on the characterization and antioxidant properties of biodegradable alginate films containing ginseng extract, J. Food Eng., 98 (2010) 377–384.
[17] L. Zhu, L. Zhang, Y. Tang, D. Ma, J. Yang, Synthesis of kaolin/sodium alginate-grafted poly(acrylicacid-co-2acrylamido-2-methyl-1 propane sulfonic acid) hydrogel composite and its sorption of lead, cadmium, and zinc ions, J. Elastomers Plast., 47 (2015) 488–501.
[18] F. Karkeh-abadi, S. Saber-Samandari, S. Saber-Samandari, The impact of functionalized CNT in the network of sodium alginate-based nanocomposite beads on the removal of Co(II) ions from aqueous solutions, J. Hazard. Mater., 312 (2016) 224–233.
[19] M. Khajeh, S. Laurent, K.D. Chem, Nanoadsorbents: classification, preparation, and applications (with emphasis on aqueous media), Chem. Rev., 113 (2013) 7728–7768.
[20] D. Liu, Z. Li, Y. Zhu, Z. Li, R. Kumar, Recycled chitosan nanofibril as an effective Cu(II), Pb(II) and Cd(II) ionic chelating agent: adsorption and desorption performance, Carbohydr. Polym., 113 (2014) 469–476.
[21] J. Abdi, M. Vossoughi, N. Mohammad Mahmoodi, I. Alemzadeh, Synthesis of metalorganic framework hybrid nanocomposites based on GO and CNT with high adsorption capacity for dye removal, Chem. Eng. J., 326 (2017) 1145–1158.
[22] R. Das, S.B. Abd Hamid, M.E. Ali, A.F. Ismail, M.S.M. Annuar, S. Ramakrishna, Multifunctional carbon nanotubes in water treatment: the present, past and future, Desalination, 354 (2014) 160–179.
[23] A. Bibi, S.u. Rehman, A. Yasin, Alginate-nanoparticles composites: kinds, reactions and applications, Mater. Res. Express, 6 (2019), doi: 10.1088/2053-1591/ab2016.

[24] M.I. Shahzad, K. Rajan, N. Shahzad, M. Arshad, D. Perrone, M. Giorcelli, A. Tagliaferro, Extensive growth of MWCNTs on copper substrates using various diffusion barrier layers, Diamond Relat. Mater., 82 (2018) 124–131.
[25] M.I. Shahzad, M. Giorcelli, D. Perrone, A. Virga, N. Shahzad, P. Jagdale, M. Cocuzza, A. Tagliaferro, Growth of vertically aligned multiwall carbon nanotubes columns, J. Phys. Conf. Ser., 439 (2013), doi: 10.1088/1742-6596/439/1/012008.
[26] A.I. Piston, A. Ferlazzo, M. Lanza, C. Milone, D. Iannazzo, A. Piperno, E. Piperopoulos, S. Galyagno, Morphological modification of MWCNT functionalized with HNO_3/H_2SO_4 Mixtures, J. Nanosci. Nanotechnol., 12 (2012) 5054–5060.
[27] C.H. Lee, Y.C. Bae, Effect of surfactants on the swelling behaviors of thermosensitive hydrogels: applicability of the generalized Langmuir isotherm, RSC Adv., 6 (2016) 103811–103821.
[28] S.G. Muntean, M.A. Nistor, E. Muntean, A. Todea, R. Ianoş, C. Păcurariu, Removal of colored organic pollutants from wastewaters by magnetite/carbon nanocomposites: single and binary systems, J. Chem., 2018 (2018) 1–16.
[29] D.L. Pavia, G.M. Lampman, G.S. Kriz, Introduction to Spectroscopy: A Guide for Students of Organic Chemistry, W.B. Saunders Co., Philadelphia, 1979.
[30] A. Nasrullah, A.H. Bhat, A. Naeem, M.H. Isa, M. Danish, High surface area mesoporous activated carbon-alginate beads for efficient removal of methylene blue, Int. J. Biol. Macromol., 107 (2018) 1792–1799.
[31] D. Kulig, A. Zimoch-Korzycka, A. Jarmoluk, K. Marycz, Study on alginate-chitosan complex formed with different polymers ratio, Polymers, 8 (2016), doi: 10.3390/polym8050167.
[32] C.Y. Ou, C.H. Zhang, S.D. Li, L. Yang, J.J. Dong, X.L. Mo, Thermal degradation kinetics of chitosan-cobalt complex as studied by thermogravimetric analysis, Carbohydr. Polym., 82 (2010) 1284–1289.
[33] S.C.M. Fernandes, C.S.R. Freire, A.J.D. Silvestre, N.C. Pascoal, A. Gandini, L.A. Berglund, L. Salmen, Transparent chitosan films reinforced with a high content of nano-fibrillated cellulose, Carbohydr. Polym., 8 (2010) 394–401.
[34] Q. Li, J. Yu, F. Zhou, X. Jiang, Synthesis and characterization of dithiocarbamate carbon nanotubes for the removal of heavy metal ions from aqueous solutions, Colloids Surf., A, 482 (2015) 306–314.
[35] S. Yang, L. Wang, X. Zhang, W. Yang, G. Song, Enhanced adsorption of Congo red dye by functionalized carbon nanotube/mixed metal oxides nanocomposites derived from layered double hydroxide precursor, Chem. Eng. J., 275 (2015) 315–321.
[36] S. Chatterjee, M.W. Lee, S.H. Woo, Adsorption of Congo red by chitosan hydrogel beads impregnated with carbon nanotubes, Bioresour. Technol., 101 (2010) 1800–1806.
[37] A. Bibi, S.u. Rehman, R. Fiaz, T. Akhtar, M. Nawaz, S. Bibi, Effect of surfactants on swelling capacity and kinetics of alginate-chitosan/CNTs hydrogel, Mater. Res. Express, 6 (2019), doi: 10.1088/2053-1591/ab0697.
[38] Q. Du, J. Sun, Y. Li, X. Yang, X. Wang, Z. Wang, L. Xia, Highly enhanced adsorption of Congo red onto graphene oxide/chitosan fibers by wet-chemical etching off silica nanoparticles, Chem. Eng. J., 245 (2014) 99–106.
[39] S. Saber-Samandari, H.O. Gulcan, S. Saber-Samandari, M. Gazi, Efficient removal of anionic and cationic dyes from an aqueous solution using pullulan-graft-polyacrylamide porous hydrogel, Water Air Soil Pollut., 225 (2014) 2177–2191.
[40] L. Wang, A. Wang, Adsorption characteristics of Congo red onto the chitosan/montmorillonite nanocomposite, J. Hazard. Mater., 147 (2007) 979–985.